



Nano Scale Disruptive Silicon-Plasmonic Platform for Chip-to-Chip Interconnection

Designs of plasmonic photodetectors

Deliverable no.: D 4.3
Due date: 10/31/2013
Actual Submission date: 10/31/2013
Authors: UVEG, AIT
Work package(s): WP4
Distribution level: RE¹ (NAVOLCHI Consortium)
Nature: document, available online in the restricted area of the NAVOLCHI webpage

List of Partners concerned

| Partner number | Partner name | Partner short name | Country | Date enter project | Date exit project |
|----------------|-------------------------|--------------------|---------|--------------------|-------------------|
| 5 | UNIVERSITAT DE VALENCIA | UVEG | Spain | M1 | M36 |

¹ **PU** = Public
PP = Restricted to other programme participants (including the Commission Services)
RE = Restricted to a group specified by the consortium (including the Commission Services)
CO = Confidential, only for members of the consortium (including the Commission Services)

Deliverable Responsible

Organization: Institute of Materials Science, University of Valencia (UVEG)
Contact Person: Juan P. Martínez Pastor
Address: C/ Catedrático José Beltrán 2
46980 Paterna, Valencia, Spain
Phone: +34 96 354 4793
Fax: +34 96 354 3633
E-mail: martinep@uv.es

Executive Summary

In this deliverable we include four different strategies/concepts to define either plasmonic photodetection or a plasmonic enhancement in semiconductor photodetectors. After a section devoted to consider these concepts from the point of view of the state of the art and experimental evidences achieved along the project, we concentrate on photodetectors incorporating a plasmonic enhancement (electric field concentration) by particular design of the electrodes used in the photodetector architecture: (i) nanogap in a nanoantenna-like plasmonic structure and (ii) nanogap plasmonic waveguide structure. In the first case the advantage is the high electric field concentration (leading to an plasmonic absorption enhancement), if the nanogap is sufficiently small, but a very small detection area. In the second case a short nanogap distance can also determine a high plasmonic absorption enhancement (the shortest nanogap value will be limited by fabrication), but the detection area can be very large, as determined by the desired photodetector footprint.

Change Records

| Version | Date | Changes | Author |
|---------|------------|--------------|-----------------------|
| 1 | 2013-10-30 | Edition UVEG | J. P. Martínez Pastor |
| 2 | 2013-11-05 | Edition UVEG | J. P. Martínez Pastor |

INDEX

| | |
|--|-----------|
| 1. Introduction and Objectives | 4 |
| 2. Considerations about plasmonic enhancement in photodetectors | 6 |
| 3. Design of a plasmonic photodetector | |
| 3.1. Design of a plasmonic nanogap-nanoantenna photodetector | 11 |
| 3.2. Design of a nano-gap waveguide photodetector | 14 |
| 4. Conclusions | 18 |
| REFERENCES | 19 |

1. Introduction and objectives

A signal generated at the plasmonic transmitter chip (laser plus modulator) has to be measured by a plasmonic receiver in order to be processed electronically. For this purpose, the receiver needs to accomplish the following conditions. The incoming signal (Surface Plasmon Polariton or photons after the metal waveguide) in the detector will be transformed into an electrical signal. The photodetector will be designed in such a way that can be compatible with a silicon substrate [1], as illustrated in Fig. 1.

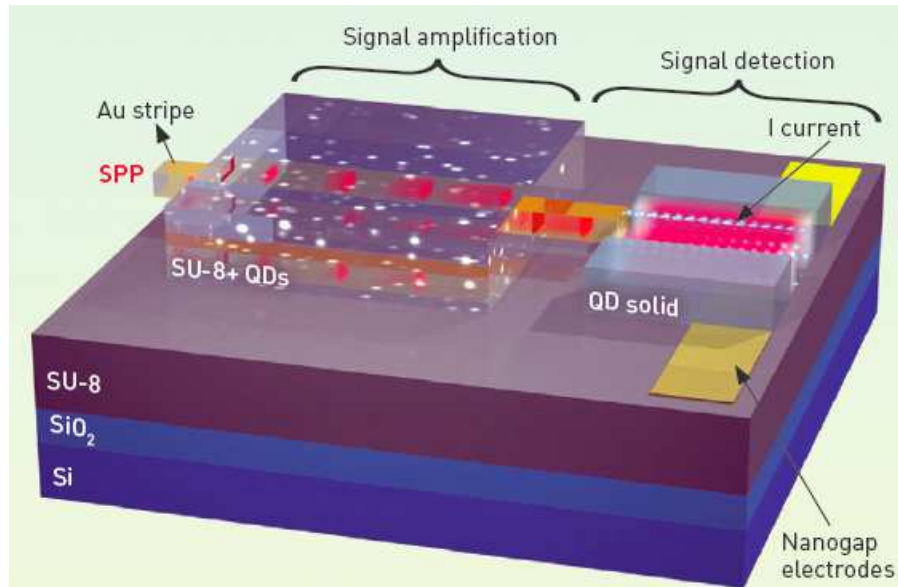


Figure 1: Plasmonic receiver with SPP amplifier and a photodetector (from Ref. 1).

The photodetector (on the right of Fig. 1) will presumably consist of a conductive layer of PbS (or other colloidal nanocrystal) quantum dots (QDs), whose thickness will be optimized to assure the maximum responsivity of the device, able to generate an electrical current as a response of the incoming photons [2]. Reported photoconductive responsivities in recent literature are in the range of 0.1-3.9 A/W for a PbS QD monolayer in a nanogap-electrode structure [3], larger than 100 A/W in the case of microgap-electrode structures with PbS layers thicker than 200 nm [4] and more than 10^6 A/W in a MOS microgap-structure based on a PbS layer (60-80 nm thick) on graphene [5]. The so-called QD-solid (conductive layer of QDs) approximation is considered one of the latest advanced concepts for photodetection, given the high absorption of quantum dots, the low cost of the solution processing technique used to deposit the material, as well as its integration in Si technology. Furthermore, this concept can be easily combined with plasmonic layers based on metal nanoparticles, because an enhancement of the responsivity is expected due to light trapping effect at the band edge of the QD-solid [4].

To achieve the goals proposed in Navolchi, we have addressed:

- 1) Synthesis and characterization of infrared colloidal QDs (PbS and PbSe). Once achieved good photoresponse with the best-known material (PbS with an effective wavelength

edge absorption around 1000 nm), as reported in D4.2, *we are focusing in the synthesis of these materials with edge absorption beyond 1500 nm (included in MS23).*

- 2) Preparation and characterization of QD-solids based on PbS (or PbSe). Previous work (D4.2) was done by using layer-by-layer method for ligand exchange after single layers (20-30 nm thick) deposited by spin-coating thin films, in order to form conductive thin films of those QDs whose thickness was in the range of 200-400 nm (MS20). However, thicker films were hard to be processed and high surface roughness was measured that can be the origin of the series resistance limitation observed in Schottky photodetector devices (see MS20). *At the moment we are working on the deposition by using blade-capillary deposition of the QD solution prior to the ligand exchange process (layer-by-layer method) to obtain films thicker than 400 nm with smaller surface roughness, other than saving in the final quantity of material (included in MS23).*
- 3) Optimization of electrical properties of conductive QD-solid films by studying Schottky photodiodes and micro-gap photoconductors (MS20). *At the moment we work on this optimization by using target material (point 1) and improving film quality and larger range of thickness (point 2), as will be reported in MS23.*
- 4) *Investigation of plasmonic effects on different photodetector architectures. This will be the subject of the present deliverable.*

In next section we will discuss, on the basis of the own research developed until now and available literature (actually a few papers that it is telling us the difficulty/challenge of the subject), the four main effects we were pursuing and advantages/disadvantages of each one:

- i) Electromagnetic (near-)field enhancement when two metal (Au, Ag) tips are very close. This was called in the project proposal as a nanogap photodetector.
- ii) Metal scatterers (spherical Ag or Au nanoparticles, for example) as a layer beneath/above the QD-solid film. In this effect, near field absorption enhancement at the QD-solid is also contemplated. This approach can be integrated in both Schotky and photoconductor designs. However, accurate experiments of this nature have been made in our group in collaboration with a group expert in photovoltaic devices and does not seems to present any advantage as compared with standard antireflective coatings. On the other hand, it is an easy way to increase light trapping in the photodetector device in a simple way without the use of additional layers affecting its electrical architecture.
- iii) Carrier-injection (tunnelling, thermoionic) from metal nanoparticles towards a conductive layer. This effect was the one pursued by using conductive polymers, as a direct way to detect Surface Plasmon Polaritons (SPP).
- iv) Waveguiding effect in a nanogap Metal-Insulator-Metal (MIM) structure, where the Insulator is a very thin nanogap region to be filled with the QD-solid. This is a new possibility (i.e., not contemplated at the beginning of the project) to increase the area occupied by QDs and hence to improve the electrical signal of the photodetector making use of this effect.

2. Considerations about plasmonic effects in photodetectors

i) Electromagnetic (near-)field enhancement when two metal tips are very close

When the density of photonic integrated circuits increases, it becomes necessary to detect optical signals with nanometer/micrometer resolution, as well as preserving on-chip integration density. Hence, photodetection devices are critical for integration of nanophotonics with electronics. The use of optical-antenna structures [6] together to colloidal QDs [2-5] are promising candidates for photodetection in nanophotonic integrated circuits. In the last years, a few examples of nanoscale QD-plasmonic photodetectors (see Fig. 2(a)) have been reported [3,7,8].

These nanoscale QD photodetectors that can easily be integrated with other photonic components, as a QD based waveguide (see Fig. 2(b)) [9]. Colloidal QDs are placed between the two electrodes spaced with a nano-gap, so that electrons can tunnel between the electrodes through the QDs. Electron transport between QDs can be considered as a problem of hopping between localized states. Carriers with higher energies have a higher probability of tunneling through the QDs and contributing to the tunneling current. This makes difficult to use this photodetector device for absorption of light at the QD effective bandedge and conductive layers of QDs for electrons/holes are needed. Fabrication of the nano-gap electrodes can be performed by using high-resolution EBL that would enable a nanogap width of around 50 nm or less: in Ref. 7 a width of 12 nm is achieved (Fig. 1(b)). These QD photodetectors can be fabricated on a silicon and hence integration with other nanophotonic devices are possible. The main advantage of the nanoscale QD photodetector lies in its high sensitivity, small size and spatial resolution, other than allowing its integration with sub-diffraction photonic waveguides. However, these advantages are taking place at expenses of a low responsivity due to its small active volume and carrier transport (tunneling). This is the reason why a new option is proposed below (effect iv listed in the introduction), i.e., increasing the active volumen to increase responsivity. Detailed plasmonic simulations will be presented for both options in next section.

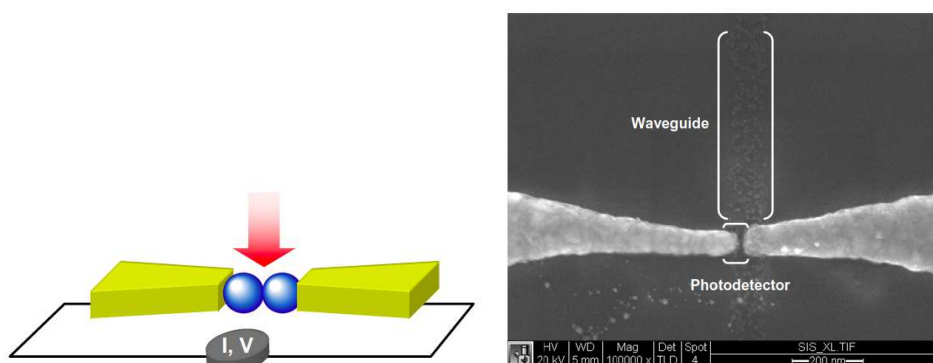


Figure 2: Illustration of a nanogap photoconductor (left) and SEM image of a fabricated waveguide-photoconductor structure (right), from Ref. 9.

ii) Metal scatterers as a layer beneath/above the QD-solid film

During the past years, extensive studies have been undertaken to investigate the use of metal nanostructures, which support localized surface plasmons, for achieving enhanced light absorption in solar cells (see for example Ref. 10 and references therein), particularly based on

Si. In particular, the deposition of metal (Ag, Au) nanoparticles (NPs) on the front surface of silicon solar cells increases the incident light trapping in Si and hence the solar cell efficiency, because the preferred light scattering by the NPs to the direction of a material with a higher dielectric constant, that is, to silicon. However, a careful analysis of the literature reveals that the data and conclusions of practically all studies in this area can hardly be applied to real solar cells which are typically already optimized in terms of light trapping by antireflection coating and/or surface texturing. That is, the increase of light trapping in Si absorbers due to metal NP deposition was observed only in a comparison with solar cells before the deposition of metal nanoparticles (bare Si surfaces). The mechanisms responsible for the light trapping increase in the silicon substrate after deposition of noble metal include [10]: (1) the forward light scattering into the silicon as a material with higher refractive index, (2) light trapping and (3) the near field enhancement around metal NPs due to excitation of localized plasmons. Recently, we demonstrated that Au NPs embedded in TiO₂, a material typically used as an antireflective coating (ARC) in Si technology, is not increasing the efficiency of the cell over the use of a film with the similar morphological characteristics and same thickness, but without the presence of Au NPs [11].

The same principles and mechanisms applies for our photodetector concept, but, of course, metal NPs will be a good substitute of an ARC, in the sense of increasing the absorption at the active film and hence photocurrent, added to a possible advantage of the near field absorption enhancement at the QD-solid film in both cases, metal NPs deposited beneath and above the QD-solid. The effect was demonstrated in Ref. 4, where the scattering by embedded Ag MNPs in the PbS QD film (see illustration in Fig. 3-left) offered a broadband responsivity enhancement in the photoconductivity. A maximum 2.4-fold photocurrent enhancement factor was obtained near the PbS-QDs bandgap (see Fig. 3), which is attributed to increased absorption due to scattering from metal nanoparticles into trapped modes inside the (dielectric) PbS QD film.

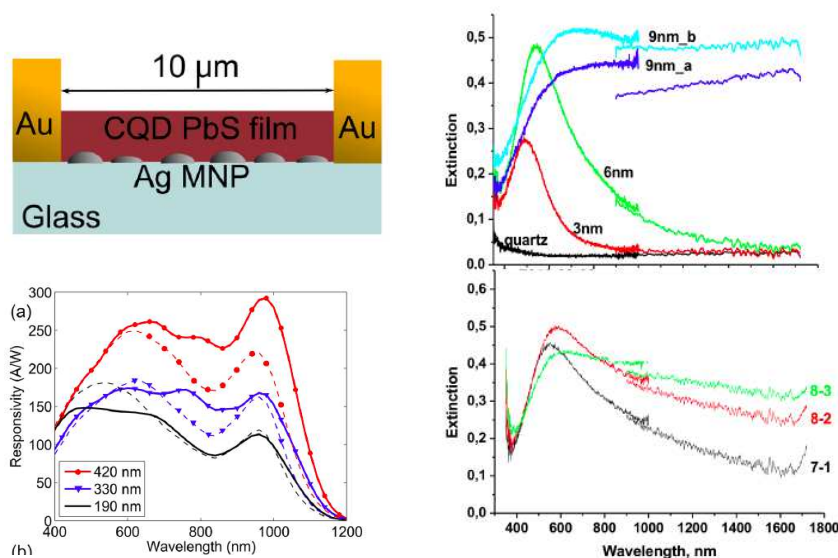


Figure 3: (Left) Illustration of a microgap photoconductor incorporating silver nanoparticles beneath the QD-film and measured responsivity with (continuous curves) and without (dashed curves) the metal nanoparticles, from Ref. 4. (Right) Experimental extinction spectra of nanometric metal layers produced by thermal evaporation of silver on glass and quartz (experimental data for the present project).

Microgap photoconductors are an alternative good option instead of nanogap photoconductors,

because of design simplicity (standard photoconductor without plasmonic enhancement in the sense explained in point i), by only taking into account the absorption coefficient of the QD-solid to estimate its appropriate thickness and distance between contacts. However, given that light from the plasmonic amplifier will be in the same plane as the photodetector, as illustrated in Fig. 1, the plasmonic light trapping effect will be more difficult to be simulated. After the optimization of the QD-solid layer at 1550 nm (current work) and the fabrication of appropriate microgap photoconductor (numbers below) the experimental evidence of improvement will be corroborated. As explained above the photocurrent would be similar to the use of an ARC and/or incorporate a surface nanostructuring, but the metal layer deposition could be made by means of a solution-processing technique, as the QD solid.

The deposition of nanometric layers of silver nanoparticles can be easily achieved by thermal evaporation, as demonstrated in Fig. 3-right using our facilities. As observed, the localized surface plasmon resonance shifts to the red by increasing the average deposited thickness of the Ag layer, other than a broadening towards long wavelengths. On the one hand, above 8 nm of Ag deposited thickness, the extinction spectrum (absorption plus scattering contributions) becomes nearly flat for wavelengths longer than 700 nm. On the other hand, the absorption coincides with extinction at the plasmon resonance and around 90 % at the near infrared region. This means that formed Ag islands are rather small (absorption dominates) and forming aggregates (shift of the plasmon resonance to the red), simultaneously. This issue can be easily solved by performing an annealing process of the layers, as suggested in Ref. 4 and other works, in order to promote coalescence of small nanoparticles in the aggregates. In this way big single Ag islands will be obtained and light scattering will be the dominant mechanism for the annealed Ag layer. This deposition and annealing is previous to deposition of QD-films and deposition of electrodes, thus ready to be applied in brief for microgap photoconductors (*).

(*) Taking into account: (i) the absorption coefficient of PbS (PbSe) QDs of appropriate size to have the ground exciton transition at around 1550 nm is around 10^4 cm^{-1} and (ii) drift mobilities in the QD-solid better than $10^{-4} \text{ cm}^2/\text{Vs}$, efficient micro-gap photoconductors would be obtained by incorporating QD films 500-1000 nm thick (to have light absorption percentage around 40-70 %) and microgap distances in the range 1-10 μm (to obtain electric fields above 10^4 V/cm and small transit times).

iii) Carrier-injection from metal nanoparticles towards a conductive layer

A more recently studied effect in literature (later than proposed in Navolchi) is the one related to the energy transfer from optically excited metal nanoparticles that can be transferred to electrons, which either overcome the metal semiconductor energy barrier or tunnel through it to become conduction electrons in the semiconductor. This effect was demonstrated recently in a TiO_2/Au composite [12]. It was measured a significant additional photoconductance when illuminated by light with photon energies well below the band gap (see Fig. 4). This photoconductance is found to track the plasmonic absorption/extinction spectrum of the Au NPs embedded in the TiO_2 semiconductor and ascribed to both to quantum tunneling of hot electrons from the metal directly into the conduction band of the TiO_2 and to energetic electrons going over the barrier transport. As reported in this work, the expected responsivity is not high and surely highly dependent on the density of metal nanoparticles inside the semiconductor. This option will be considered in next future experiments using conducting polymers in microgap photoconductors, but simulations are very complicate at this stage given the aforementioned electronic mechanisms.

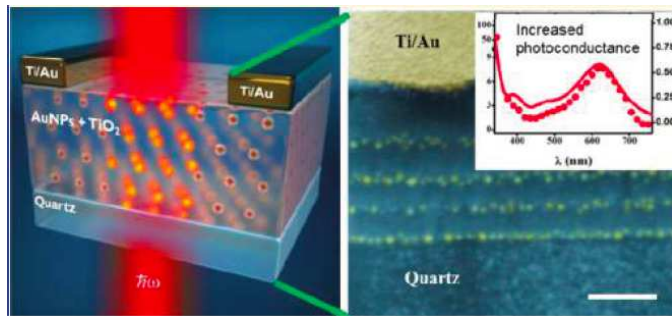


Figure 4: Illustration of a TiO_2/Au nanocomposite photoconductor and measured photoconductance below the bandgap of TiO_2 due to the plasmon absorption by Au nanoparticles, from Ref. 12.

iv) Waveguiding effect in a nanogap Metal-Insulator-Metal (MIM) structure

This option was proposed as a way to increase the detection area in the plasmonic photodetector as compared to a nanoantenna concept, where this area is extremely small and thus limiting the maximum quantity of QDs absorbing light and the corresponding photocurrent. The gap plasmon waveguide (GPW) [13] is particularly interesting, because its modes are extremely small and its fabrication process is comparably simple. The excitation of GPW modes will be possible by external radiation (Fig. 5) and end-fire coupling (Fig. 6), as also corroborated in section 3.1. A more efficient coupling to modes of GPW is achieved by using nanoantennas (Fig. 5) [14], because of the high light concentration by them, which can be the analogous case of the coupling between plasmonic waveguides and the photoconductor at the receiver (Fig. 1). In the example intensity enhancement inside the waveguide is around 400 relative to the incident beam when exciting with the resonant nanoantenna compared to less than 4 without nanoantennas.

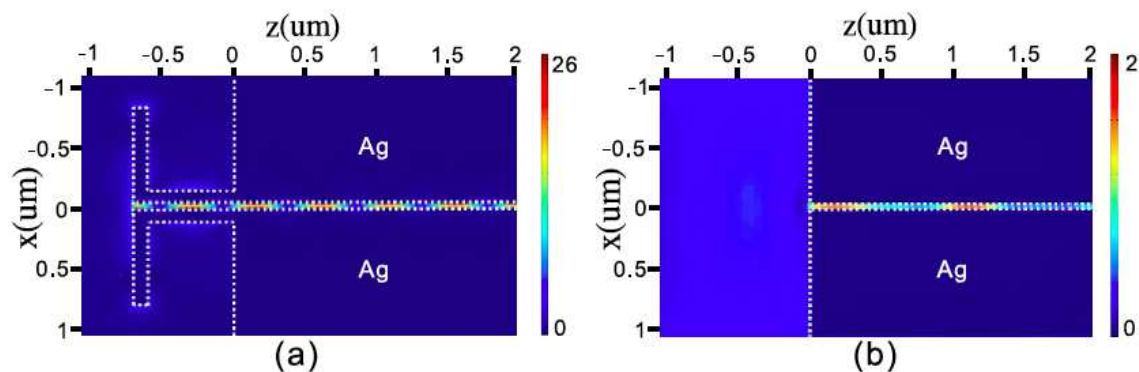


Figure 5: Field distributions on the plane of a GPW (gap = 30 nm), when exciting with (a) and without (b) an antenna, from Ref. 14.

It is worth noting the case of a GPW with tapered and direct end-fire coupling (Fig. 6) [15]. The tapered coupling efficiency is $\sim 80\%$ (2D FDTD simulation) even when input/output waveguide dimension ratio was 20 and even though the “diffraction limit” point was crossed in the taper toward the nanoscale. More surprising is the highly efficient direct coupling, which exceeds significantly the propagating modes overlap. This can be interpreted by a similar mechanism generating the enhanced harvesting in a hole array made on a metal layer where super-transmission takes place [16].

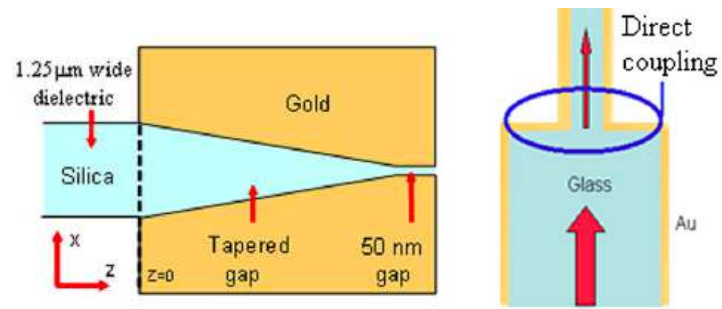


Figure 6: Coupling between a core optical fibre into a MIM gap: tapered (left) and direct (right), from Ref. 15.

3. Design of a plasmonic photodetector

The 3D simulations of the different considered cases have been developed by using COMSOL software based on the Finite Element Method.

3.1. Design of a plasmonic nanogap-nanoantenna photodetector

The bowtie nanoantenna is defined on top a silica substrate ($n = 1.51$) and surrounded by air. The real and imaginary refractive indices of gold are taken from an interpolation with splines of the experimental data obtained by Palik *et al.* [17]. The bowtie nanoantenna is a triangular prism with 120 nm of side length, a height of 50 nm and vertices with a radius of curvature of 15 nm, in order to avoid divergences.

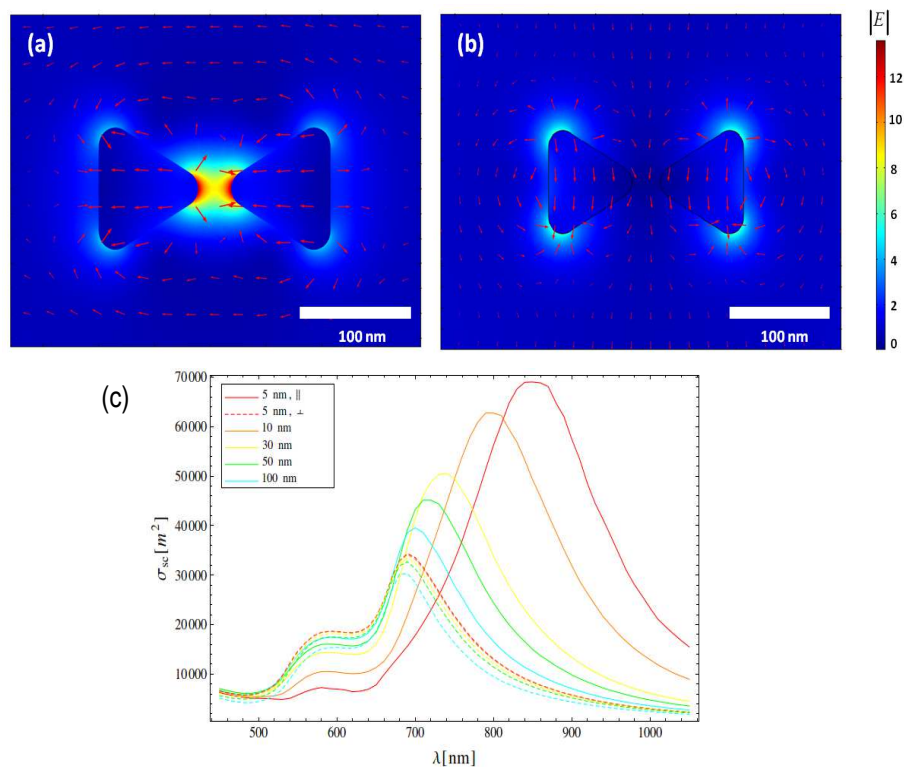


Figure 7: Distribution of electric field at 780 nm in the plane of a bowtie nanoantenna (gap distance = 30 nm) along the direction parallel (a) and perpendicular (b) to its gap major axis; (c) Scattering cross-section as a function of the wavelength.

A scattering mode with a background field was introduced as an analytic expression; in the model, two semi-infinite media (water and air) are used so the background field is defined as the sum of the incident and reflected wave in the first media and the transmitted wave in the second media through the use of the Fresnel equations. This allows us to extract the scattered fields without the need of two simulations, one to calculate numerically the background field and the other to compute the scattered field.

We have placed PMLs (Perfect Matched Layers, which are domains with the same refractive index as the surrounding domains at their boundary but with increasing imaginary refractive index when moving away from it) and SBC (Scattering Boundary Conditions, boundaries

transparent for scattered waves) around the entire physical domain. These boundary conditions result in the absorption of the EM waves that arrive at the boundaries of our physical domain, preventing unphysical reflections.

When simulating the light interaction with the nanostructure the electromagnetic field distribution is derived directly from solving the problem in terms of the fields within the simulated domains and absorption cross-sections can be obtained from the integration of the resistive heat generation over the volume of the nanoantenna. The scattering cross-sections are derived from the integration of the Poynting vector (from the consideration of energy conservation):

$$\sigma_{sc} = \frac{1}{2I_0} \int (\mathbf{E}_{sc} \times \mathbf{H}_{sc}) \cdot d\mathbf{S}$$

over a surface that surrounds the nanoantenna, extinction cross-sections are then the sum of the scattering and absorption cross-sections.

As expected, an incident linearly polarized wave with electric field parallel to the major axis of the bowtie (perpendicularly to its plane) results in a high confinement of electric field within the gap region of the nanoantenna with a gap distance of 30 nm (Fig. 7 (a)). If the polarization is perpendicular, the enhancement regions are located around the other tips of the bowtie (Fig. 7 (b)), far from the gap region, and the enhancement factor becomes considerably lower.

Along the direction parallel to the major axis of the bowtie an increasing redshift and bandwidth of the more intense and longer wavelength plasmon resonance is observed by diminishing the gap distance (Fig. 7 (c)), contrary to the perpendicular case (shorter wavelength plasmon resonance), where the redshift is practically absent. These resonant plasmonic modes at short and long wavelengths are characteristics of the single particle and dimmer of the bowtie, respectively, and calculated scattering cross-section is consistent with extinction efficiency and transmission data for similar nanoparticles modelled elsewhere [18]. The maximum shift of the long wavelength (longitudinal) plasmon resonance associated to the bowtie dimmer is found when both prism nanostructures are touching and hence constituting a new single metal nanostructure. By increasing the prism size further tuning of the longitudinal plasmon mode can be achieved, but the effect of electric field concentration at the bowtie gap will be not very different at the broad wavelength range defined by this mode. This effect is mainly determined by the reduction of the bowtie gap distance, when the evanescent electric field perpendicular to each metal nanostructure overlaps, as observed in Figs. 8 and 9. Accordingly, when the bowtie gap distance is sufficiently small the electric field enhancement increases notably (Fig. 9).

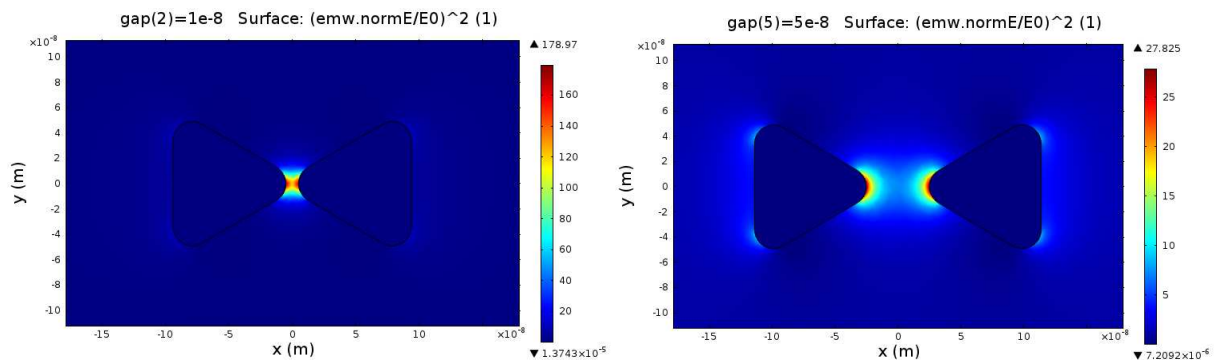


Figure 8: Distribution of electric field intensity at 1550 nm in the plane of a bowtie nanoantenna along the direction parallel to its gap major axis for gap distance of 10 and 50 nm.

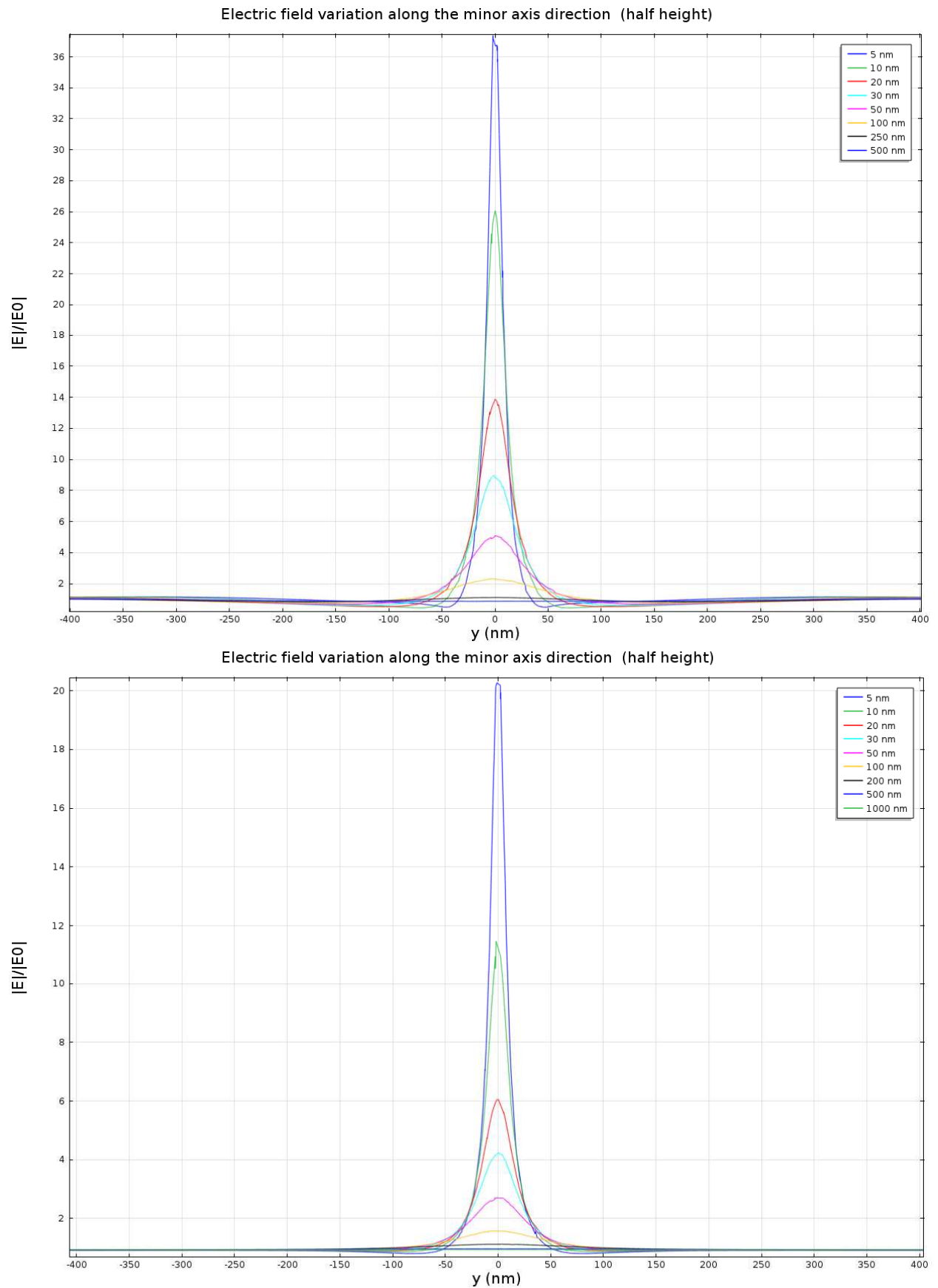


Figure 9: Electric field enhancement at 780 (top panel) and 1550 (bottom panel) nm along the direction perpendicular to the gap major axis of the bowtie nanoantenna for several gap distances.

The extension of the zone with enhanced electric field along the perpendicular direction of the bowtie gap major axis broadens with increasing the gap distance, as observed in Fig. 9. For a gap distance of 30 nm the electric field enhancement is 4 (16 for the intensity enhancement) and its extension across the gap around 40 nm, i.e., thus the total area will be 1800 nm^2 (total volume to be occupied by QDs about $9 \times 10^4 \text{ nm}^3$ that means 2500 QDs of radius 3 nm in total), approximately. Evidently, this small number of QDs for (enhanced) absorption of light will determine the maximum photocurrent delivered by the photoconductor. On the other hand, enhanced absorption, as also the incident total number of photons, means a higher rate of produced electron-hole pairs at the QDs, but it does not necessarily lead to a proportional photocurrent increase due to losses by Auger non radiative recombination. Finally, the fabrication of the photodetector will define enlarged metal structures on the opposite sides of the nanogap and hence a much broader resonance for the longitudinal plasmon mode, but still remaining the electric field concentration effect, as discussed above.

3.2. Design of a nano-gap waveguide photodetector

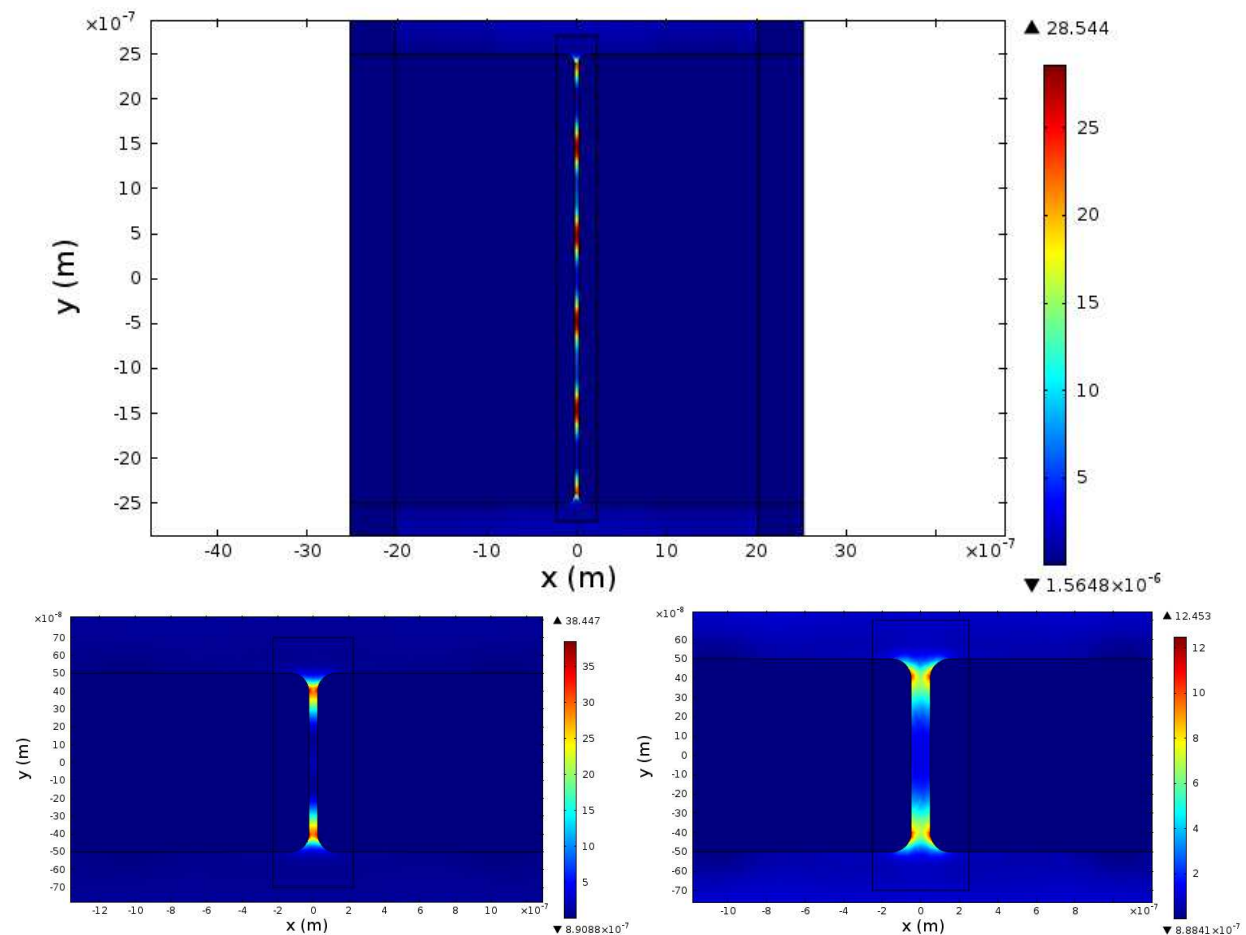


Figure 10: Distribution of electric field intensity at 1550 nm in a nano-GPW 5 μm long and gap distance equal to 50 nm (top panel); idem for a GPW 1 μm long (bottom panel) with gap distances of 50 (bottom-left) and 100 (bottom-right) nm.

Some characteristic simulations of the electric field intensity distribution in a nano-GPW are presented in Fig. 10 by considering light under normal incidence (linearly polarized perpendicular to the gap slot). Clearly, the electric field concentrates in the gap region and several intensity maxima are observed, depending on the nano-GPW length in agreement with simulations elsewhere (see references cited in section 2). This is what we were suggesting in the last paragraph, regarding the size of the metal electrodes at opposite sides of the nanogap, even if now a qualitative difference arises: a surface plasmon polariton standing wave develops when increasing the length of the nano-GPW in contrast to the localized nature of the surface plasmon in the bowtie nanoantenna. Of course the intensity enhancement inside the nano-GPW is highly dependent on gap distance, a three-fold decrease when increasing the gap from 50 to 100 nm (bottom panel of Fig. 10). In contrast, the electric field enhancement is very similar in 1 and 5 μm long nano-GPW, as can be better observed in Fig. 11 (top panel). For other wavelengths (1 and 2 μm were analysed) the electric field enhancement does not seem to be very different (Fig. 11), at least for a 5 μm long nano-GPW. For short nano-GPW (see the electric field distribution for 500 nm length in Fig. 11) it is possible a more complex situation, intermediate from localized to propagating surface plasmons when the wavelength is greater/equal than the nano-GPW length. A deeper theoretical analysis could be needed in these cases to corroborate if the COMSOL simulation is correct. In the case of wavelength smaller than the nano-GPW length the simulation should be good, because a long range SPP is propagating with very reduced losses (in the infrared region), i.e., attenuation seems to be negligible along the gap-waveguide length. Finally, the simulation of the electric field amplitude/intensity on the nano-GPW by coupling in-plane travelling light (plane wave) is shown in Fig. 12, by considering a semi-infinite nanogap waveguide (PML conditions on the right side of the structure). The results are not very different from those discussed before in the case of vertical incidence, that is, the surface plasmon polariton propagates inside the nano-GPW without appreciable losses. The entrance to the nano-GPW is considered tapered-like instead of abrupt, but not big differences are expected for this case, as discussed in section 2, despite a slight reduction in the coupling efficiency.

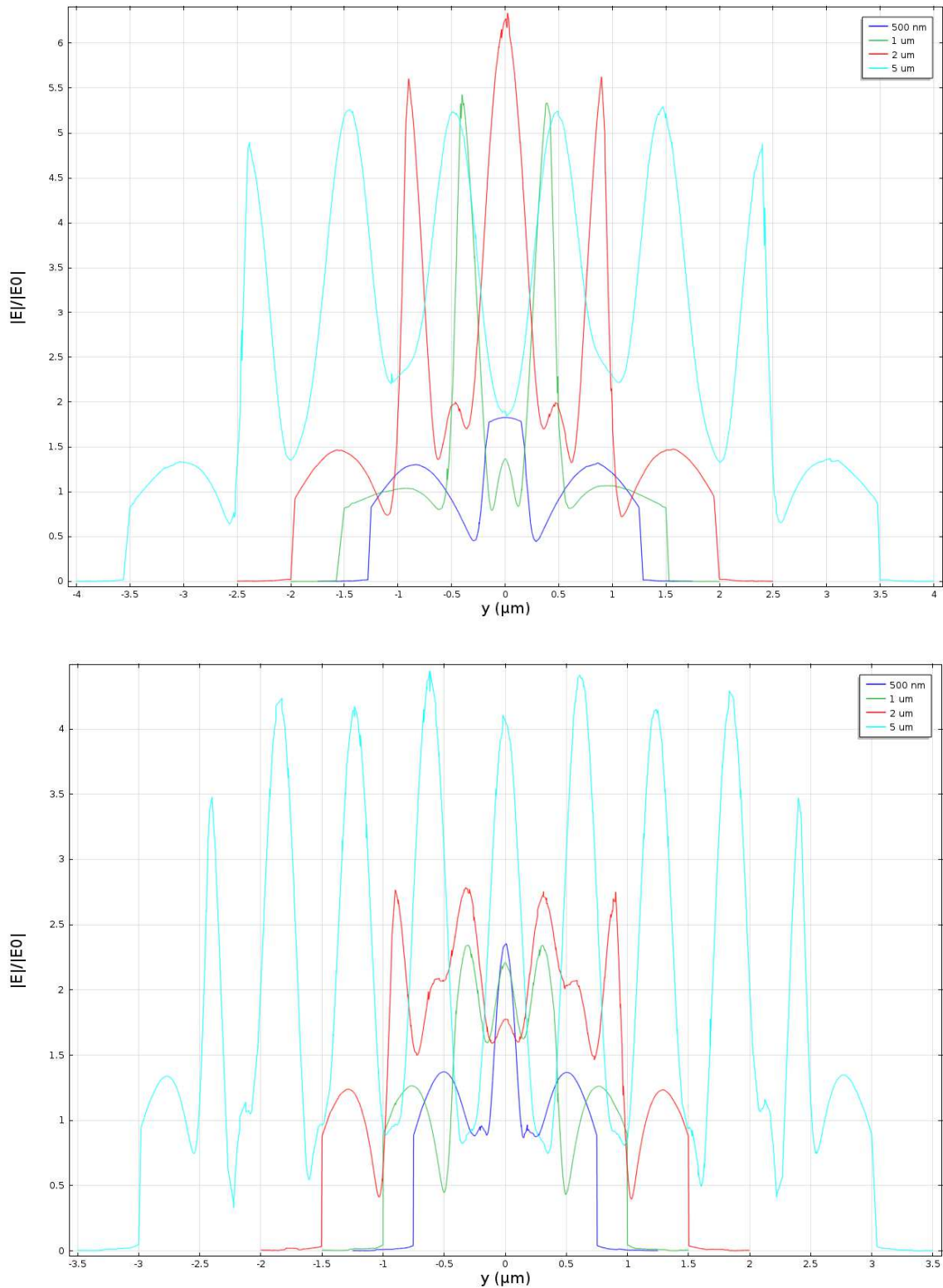


Figure 11: Electric field variation at 1550 (top panel) and 1000 (bottom panel) nm in a nano-GPW of different lengths (the gap distance is fixed to 50 nm).

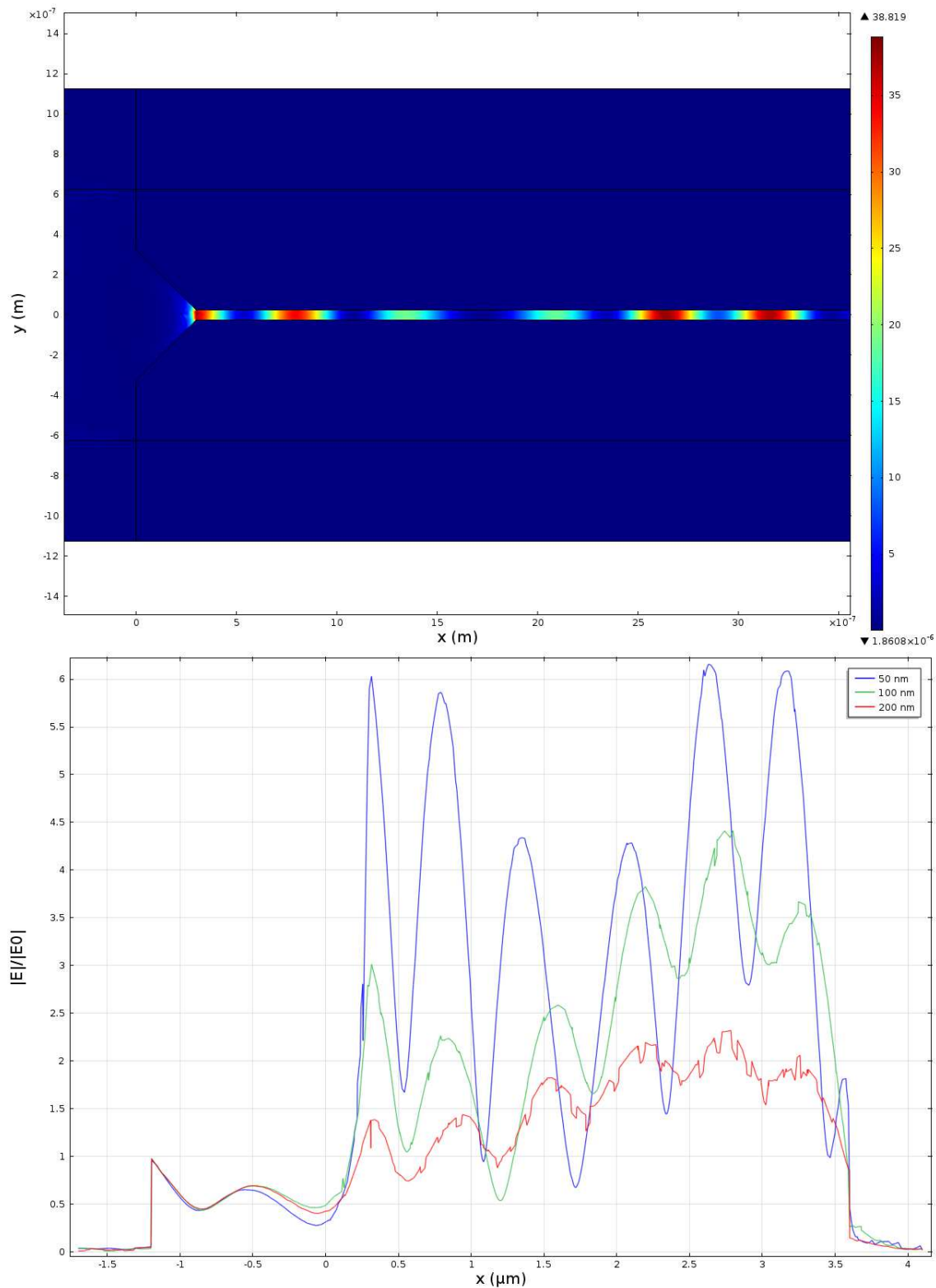


Figure 12: Distribution of electric field intensity at 1550 nm in a nano-GPW 5 μm long and gap distance equal to 50 nm (top panel) by coupling in-plane light (planar wave from the left); Electric field variation in the same GPW for different lengths.

7. Conclusions and outlook

In this deliverable we include four different strategies/concepts to define either plasmonic photodetection or a plasmonic enhancement in semiconductor photodetectors. Two of these concepts does not involve simulations, other than work developed until now and further experimental work. Therefore, in section 3 we have concentrated on simulations of photodetectors incorporating a plasmonic enhancement (electric field concentration) by particular design of the electrodes used in the photodetector architecture:

- (i) nanogap in a nanoantenna-like plasmonic structure and
- (ii) (nanogap plasmonic waveguide structure.

In the first case the advantage is the high electric field concentration (leading to an plasmonic absorption enhancement), if the nanogap is sufficiently small, but a very small detection area. In the second case a short nanogap distance can also determine a high plasmonic absorption enhancement (the shortest nanogap value will be limited by fabrication), but the detection area can be very large, as determined by the desired photodetector footprint. Here the electrodes, which are parallel to the nanogap slit, length is considered for fabrication in the range from 2 to 5 μm in order to absorb most of the light coming from the plasmonic amplifier.

Next work (most of the efforts will be concentrated at short time on points 1-2 and 3 in parallel):

- 1) Continue with some more simulations incorporating the complex dielectric constant of the semiconductor (PbS QD-solid). More precise modelling (mainly focused on the estimation of coupling efficiency by using a point source in the plane of the gap to simulate the exit of the plasmonic amplifier and wavelength dependence) will be undertaken after successful fabrication and performance of nano-GPW photoconductors.
- 2) Fabrication layout of the nano-GPW photoconductor with nanogap as short as possible and electrode length in the from 2 to 5 μm . Process definition, fabrication and characterization.
- 3) Fabrication of microgap photoconductors by incorporating a plasmonic light-trapping layer (instead of anti-reflective coating) based on Ag droplets formed by thermal evaporation plus annealing.
- 4) Investigation of plasmon detection using semiconducting polymers.

REFERENCES

-
- [1] J. Leuthold, S. Muehlbrandt, A. Melikyan, M. Kohl, C. Koos, W. Freude, V. Dolores- Calzadilla, M. Smit, I. Suarez, J. Martínez-Pastor, E.P. Fitrakis and I. Tomkos, "Plasmonic Communications: Light on a Wire", *Optics & Photonics News*, vol. May 2013, 30-35 (2013).
- [2] G. Konstantatos and E.H. Sargent, "Nanostructured materials for photodetection", *Nature Nanotechnology* **5**, 391-400 (2010).
- [3] Ferry Prins, *et al.*: "Fast and Efficient Photodetection in Nanoscale Quantum-Dot Junctions", *Nano Lett.* **12**, 5740–5743 (2012).
- [4] F. Pelayo García de Arquer *et al.*, "Plasmonic light trapping leads to responsivity increase in colloidal quantum dot photodetectors", *Appl. Phys. Lett.* **100**, 043101 (2012).
- [5] G. Konstantatos *et al.*, "Hybrid graphene–quantum dot phototransistors with ultrahigh gain", *Nature Nanotechnology* **7**, 363-368 (2012).
- [6] J. Alda, J. M. Rico-Garcia, J. M. Lopez-Alonso, and G. Boreman, "Optical antennas for nano-phonic applications", *Nanotechnology* **16**, S230-S234 (2005).
- [7] M. C. Hegg and L. Y. Lin, "Near-field photodetection with high spatial resolution by nanocrystal quantum dots" *Opt. Exp.* **15**, 17163-17170 (2007).
- [8] M. C. Hegg, M. P. Horning, T. Baehr-Jones, M. Hochberg, and L. Y. Lin, *Appl. Phys. Lett.* **96**, 101118 (2010).
- [9] L. Huang, M. C. Hegg, C.-J. Wang, and L. Y. Lin, "Fabrication of a nanophotonic waveguide and photodetector integrated device", *Micro Nano Lett.* **2**, 103-106 (2007).
- [10] H. A. Atwater and A. Polman, *Nature Mater.* **9**, 205 (2010).
- [11] J. A. Töfflinger, E. Pedrueza, V. Chirvony, C. Leendertz, R. García-Calzada, R. Abargues, O. Gref, M. Roczen, L. Korte, J. P. Martínez-Pastor, and B. Rech, "Photoconductivity and optical properties of silicon coated by thin TiO₂ film in situ doped by Au nanoparticles", *Phys. Stat. Sol. (a)* **210**, 687–694 (2013).
- [12] S. Mubeen, G. Hernandez-Sosa, D. Moses, J. Lee, and M. Moskovits, "Plasmonic Photosensitization of a Wide Band Gap Semiconductor: Converting Plasmons to Charge Carriers", *Nano Lett.* **11**, 5548–5552 (2011).
- [13] L. Liu, Z. Han, and S. He, "Novel surface plasmon waveguide for high integration," *Opt. Express* **13**, 6645–6650 (2005).
- [14] J. Wen, S. Romanov, and U. Peschel, "Excitation of plasmonic gap waveguides by nanoantennas", *Optics Express* **17**, 5925 (2009).
- [15] P. Ginzburg, D. Arbel, and M. Orenstein, "Gap plasmon polariton structure for very efficient microscale-to-nanoscale interfacing", *Opt. Lett.* **31**, 3288–3290, (2006).
- [16] T. W. Ebbesen, H. J. Lezec, H. F. Ghaemi, T. Thio, and P. A. Wolff, "Extraordinary optical transmission through sub-wavelength hole arrays", *Nature* **391**, 667–669 (1998).
- [17] E. D. Palik, *Handbook of Optical Constants of Solids* (Academic Press, 1997).
- [18] Stephanie Dodson, Mohamed Haggui, Renaud Bachelot, Jérôme Plain, Shuzhou Li and Qihua Xiong, "Optimizing Electromagnetic Hotspots in Plasmonic Bowtie Nanoantennae", *J. Phys. Chem. Lett.* **4**, 496–501 (2013).